GISM

GLOBAL **I**ONOSPHERIC
SCINTILLATION **M**ODEL

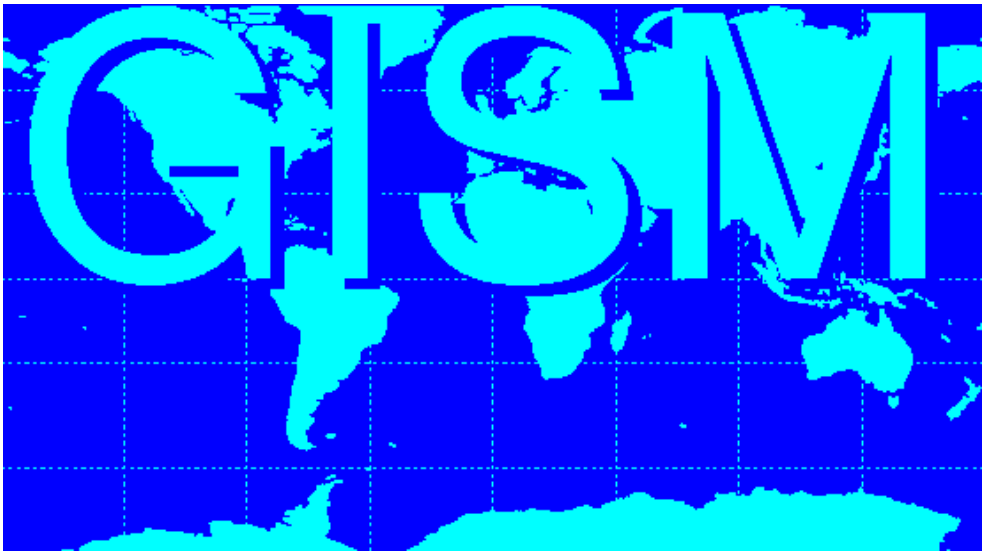

Document written by Y. Béniguel
beniguel@ieea.fr

Table of contents

1. Introduction

Ionospheric scintillations are rapid variations of phase and amplitude of a signal, which passes through the Ionosphere. They are very pronounced in equatorial regions where they appear every day after sunset and may last a few hours. They are related in particular to the solar activity and the season. The main factors whose dependency has been established are indicated hereafter. At mid-latitudes, the scintillations are rather weak, except during conditions of ionospheric storms. The scintillations result in signal degradation from VHF up to C band. They are a major issue for many systems including Global Navigation Satellite Systems (GNSS), telecommunications, remote sensing and earth observation systems.

The signal fluctuations, referred as scintillations, are created by random fluctuations of the medium's refractive index, which are caused by inhomogeneities inside the ionosphere. These inhomogeneities are sub structures of bubbles which may reach dimensions of several hundreds of kilometers as can be seen from radar observations (Costa et al, 2011). These bubbles present a patchy structure. They appear after sunset when the sun ionization drops to zero. Instability processes develop inside these bubbles with creation of turbulences inside the medium. As a result, depletions of electron density appear. In the L band and for the distances usually considered, the diffracting pattern of inhomogeneities in the range of one kilometer size, is inside the first Fresnel zone and contribute to scintillation.

The signal propagation through inhomogeneities create a number of modifications of transmitted signals among them phase and intensity fluctuations, fluctuations of the arrival angle, dispersivity, Doppler,… This problem has been studied at large in the past. The review paper published by Yeh and Liu, (1982) details the theoretical approaches and gives experimental results. Methods presented include the Rytov approximation in case of weak fluctuations, the phase screen theory and the parabolic equation (PE) method. GISM model presented in this document, uses the Multiple Phase Screen technique (MPS). It consists in a resolution of the PE for a medium divided into successive layers, each of them acting as a phase screen.

GISM model provides the statistical characteristics of the transmitted signals, in particular the scintillation index, the fade durations and the cumulative probability of the signal allowing consequently determining the margins to be included in a budget link. Maps of the scintillation index S4 and of the phase standard deviation may also be obtained.

2. Inhomogeneities characteristics

The following parameters are input parameters to the model:

- The spectral density of the electron density fluctuations named p,
- Their correlation distance L_0,
- Their velocity and direction of displacement.

GISM default values are p = 3, L_0 = 1000 m drift velocity = 100 m. / s.

Spectral density

The scintillations spectrum usually exhibits a linear variation with the logarithm of frequency. The most important parameter is the inclination index of this spectrum: p. The cut-off frequency is related to the correlation distance of inhomogeneities. In most cases, the significant part of the spectrum is between 0.1 Hz and 1 Hz.

The signal spectrum deduced from the measurements is approximated by expression Tf^{-p} which applies to most of the cases, where T, defined as the value at 1 Hz, is related to the turbulence strength. Figure 1 below shows measurement results recorded during the PRIS measurement campaign (Béniguel, 2009). The GPS week n° 377 (modulo 1024) was selected to derive the parameters p and T. Samples corresponding to S4 values greater than 0.2 were only selected in this analysis in order to diminish the receiver noise effect on the results. The slope value has a median value equal to 2.7. It decreases with time after sunset corresponding to the fact that the inhomogeneities sizes decreases with time after sunset. It should be noticed however that the PRIS measurement campaign was done in a year close to solar minimum. High solar activity values might be different, in particular for the strength.

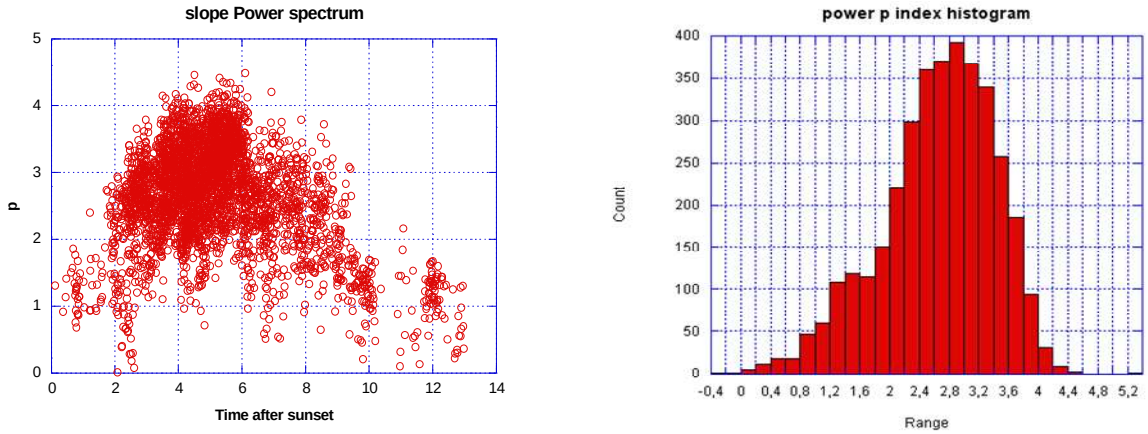

Figure 1: slope value deduced from measurements in Cayenne
(one week of 50 Hz raw data files analysis)

Correlation length

The coherence length of inhomogeneities varies with local specific conditions. To perform a propagation calculation, the medium is assumed to be statistically homogeneous and typical characteristics of the inhomogeneities are assigned to the different altitude layers used in the successive phase screens. The mean value of the correlation length deduced from measurements is about 1 km at the F layer altitude. This value is taken as default value in GISM.

Drift of the irregularities causes a Doppler shift of the diffraction pattern. Both the direction and the modulus of velocity are important and are taken into account in the characterization of the statistical properties of the medium. Typical values of the drift velocity are 100 m / s. at low latitudes and 1000 m. / s. at high latitudes.

Height of irregularities

The height at which instabilities develop may be obtained from the diffraction pattern of the transmitted signals. This last is related to the dimension of the first Fresnel zone. The corresponding frequency is obtained from the spectral density spectrum of the irregularities. This frequency being measured, the altitude where the irregularities develop is easily obtained. Histograms of measurements show a peak value at altitudes between 300 and 500 km, consequently at the F layer altitude (Afraimovitch et al, 1994), (Mc Dougall, 1981).

3. Dependency of scintillations on the latitude

Scintillations are most severe and prevalent in and north of the auroral zone and near the geomagnetic equator (Aarons, 1982). The equatorial region extends approximately from -20° to 20° and auroral regions for latitudes greater than 55°. These boundaries change with the time of the day, the season of the year, the sunspot number and the magnetic activity.

Low latitudes scintillations

Scintillation is predominantly a nighttime phenomenon in the equatorial region occurring for more than 40% of the year during the 20:00 – 02:00 local time period (Basu et al 1976). It also shows a strong seasonal dependence with a pronounced minimum at the southern solstice and relatively high scintillation activity at the northern solstice. Equatorial scintillations also show a tendency to occur more often during years in which the sunspot number is high.

Figure 2 shows measurement results of intensity scintillations (S4) (left panel) and phase scintillation (sigma phi) (right panel) recorded in Vietnam (courtesy, University of Rennes), during the PRIS measurement campaign.

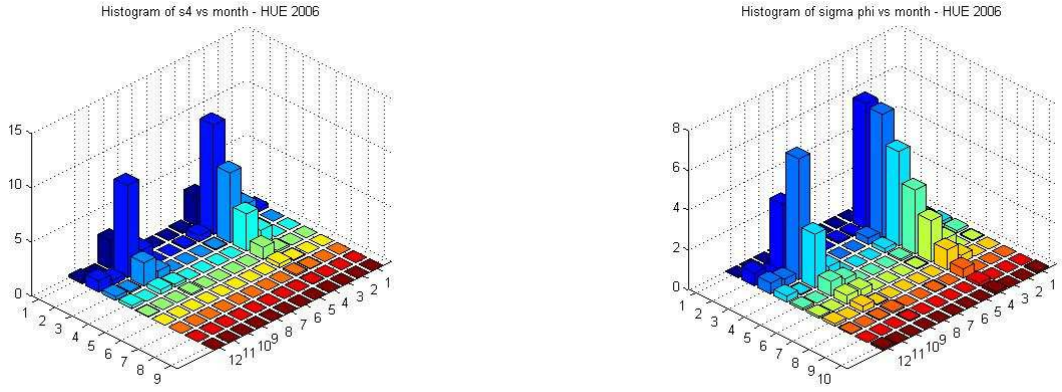

Figure 2: histogram of intensity and phase scintillations recorded in Vietnam
Horizontal axis: left panel: the value of S4 to be multiplied by 0.1; right panel: the month number
Vertical axis: normalized number of events

4. Dependency of scintillations on local time

Figure 3 (courtesy CLS, Toulouse) was obtained cumulating scintillation over a whole year. The scintillation starts after sunset and last a few hours.

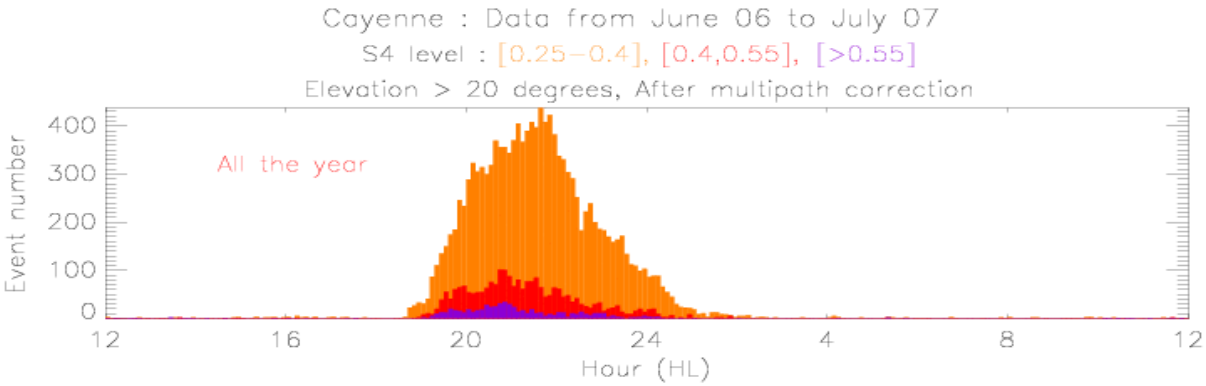

Figure 3: Distribution of one year of scintillation events June06 - July07 (6 mn intervals)

5. GISM Propagation Model

5.1 Medium modelling

The electronic density inside the medium is calculated by model NeQuick developed by the University of Graz and ICTP Trieste (Radicella, 2009). Inputs of this model are the solar flux number, the year, the day of the year and the local time. It provides the electronic density average value for any point in the ionosphere (latitude, longitude, altitude). NeQuick model is used as a subroutine in the GISM model.

The magnetic parameters are computed based on a Schmidt quasi-normalized spherical harmonic model of the magnetic field. These are the declination, the inclination, the vertical intensity and the components of the field. The code used has been developed by the National Geophysical Data Center, NOAA, Boulder, Colorado. It is used as a subroutine in the GISM code. Given the location of a point on a ray, it provides the magnetic parameters. This allows calculating the Faraday rotation.

5.2 Algorithm

GISM model uses the Multiple Phase Screen technique (MPS) (Knepp, 1983, Béniguel, 2002, 2004, Gherm, 2005). The locations of transmitter and receiver are arbitrary. The link angle of incidence is arbitrary with respect to the ionosphere layers and to the magnetic field vector orientation. It can cross the entire ionosphere or a small part of it. At each screen location along the line of sight, the parabolic equation (PE) is solved. GISM allows calculating mean errors and scintillations due to propagation through the ionosphere.

The mean errors are obtained using a ray technique solving the Haselgrove equations (Budden, 1985). The ionosphere electronic density at any point inside the medium, required for this calculation is provided by the NeQuick model. Mean errors are related to the TEC value. The range and angular errors and the Faraday rotation are calculated.

The line of sight being determined, the fluctuations are calculated in a second stage using the multiple phase screen technique. The medium is divided into successive layers, each of them acting as a phase screen. In this technique, which is detailed hereafter, the field is scattered from one screen to the next one.

The calculation is a 2D calculation. The first dimension is the line of sight previously determined and the second dimension is perpendicular to that one. Symmetry of revolution is consequently assumed.

The wave propagation is calculated solving the Helmholtz equation (Ishimaru, 1978).

$$\left[\nabla^2 + k^2 \left(1 + \varepsilon_1(\bar{r})\right)\right] u(\bar{r}, z) = 0 \qquad (1)$$

Where

- $k^2 = \omega^2 \mu_0 \varepsilon_0 \langle \varepsilon_r \rangle = k_0^2 \langle \varepsilon_r \rangle$ is the local wave number
- μ_0, ε_0 and k_0 are the free space permeability, permittivity and wave number
- $\bar{r}$ is one observation point inside the medium and z is the coordinate along the direction of propagation.

The dielectric permittivity along the main propagation axis *z*, is written:

$$\varepsilon_r(\bar{r}) = \langle \varepsilon_r \rangle \left[1 + \varepsilon_1(\bar{r}) \right] \tag{2}$$

with $\varepsilon_1(\bar{r})$ is the random part of the relative dielectric permittivity.

Introducing the complex amplitude $U(\bar{r}, z)$ of the stochastic field

$$u(\bar{r}, z) = U(\bar{r}, z) \exp\left(j \int k(z)\, dz \right) \tag{3}$$

and assuming that the variation of the complex amplitude is mainly in the direction perpendicular to the main propagation axis (parabolic approximation), the stochastic parabolic equation for the complex amplitude can be written in the form

$$2jk \frac{\partial U(\bar{r}, z)}{\partial z} + \nabla_t^2 U(\bar{r}, z) + k^2 \varepsilon_1(\bar{r}, z) U(\bar{r}, z) = 0 \tag{4}$$

where ∇_t^2 is the transverse Laplacian.

5.3 Algorithm

To solve this equation, the medium is divided into series of successive layers (or screens) perpendicular to the main propagation axis, each one being characterized by local homogeneous statistical properties. The solution is then obtained by iterating successively scattering and propagation calculations as detailed hereafter.

The parabolic wave equation is split into two equations. The first one describes the phase change due to the presence of random fluctuations $\varepsilon_1(r, z)$; r is the distance to the propagation direction main axis.

$$2jk \frac{\partial U(r, z)}{\partial z} + k^2 \varepsilon_1(r, z) U(r, z) = 0 \tag{5}$$

with solution

$$U(r, z + \Delta z) = U(r, z) \exp\left(j k \Delta z \varepsilon_1(r, z)/2 \right) \tag{6}$$

The second equation describes propagation between two screens

$$2\,jk\frac{\partial U(r,z)}{\partial z} + \nabla^2 U(r,z) = 0 \qquad (7)$$

This equation is solved in the transform domain with solution

$$U(r,\ z+\Delta z) = \int_{-\infty}^{\infty} \hat{U}(p,z)\ \exp\left(j\,p^2\,\frac{\Delta z}{2k} - j\,p\,r\right)\ dp \qquad (8)$$

The Fourier transform of the complex amplitude is calculated after the first step. It is as an input to the second step. Applying this two step technique to each successive layer, the multiple phase screens (MPS) solution of the parabolic equation is obtained (Yeh, 1977, Knepp, 1983). All these calculations can be performed using FFT techniques.

In most of the cases considered, the source point is very far away from the fluctuating medium. The incident field on the first layer is a plane wave and the initial value of the field complex amplitude on this screen is 1.

Medium synthesis

For a given layer the transmitted phase spectral density of the signal is (Rino, 1979) :

$$\gamma_{\Phi}(q) = \frac{C_p}{\left(q_0^2 + q^2\right)^{p/2}} \qquad (9)$$

with $q_0 = 2\pi / L_0$
and L_0 in meters is the average size of the inhomogeneities.

At each phase screen, the phase synthesis is performed taking the inverse Fourier transform of the product of a random numbers series with given uniform probability density by numbers with the required spectral density. This provides a series of random numbers with the required statistical properties (Picinbono, 1968).

6. Scintillations at receiver level

6.1 GPS Receiver Architecture

A GPS receiver is a spread spectrum receiver, requiring several essential parts for acquisition, tracking and extracting useful information from the incoming satellite signal. It can be broadly divided into three sections: the RF Front-end (RFF), Digital Signal Processing (DSP) and the Navigation Data Processing (NDP). The RFF and the DSP sections generally consist of various hardware modules, whereas the NDP section is implemented using software. Figure 4 shows a simple block diagram of a typical single frequency GPS receiver with major interfaces and input/output signals of the essential blocks.

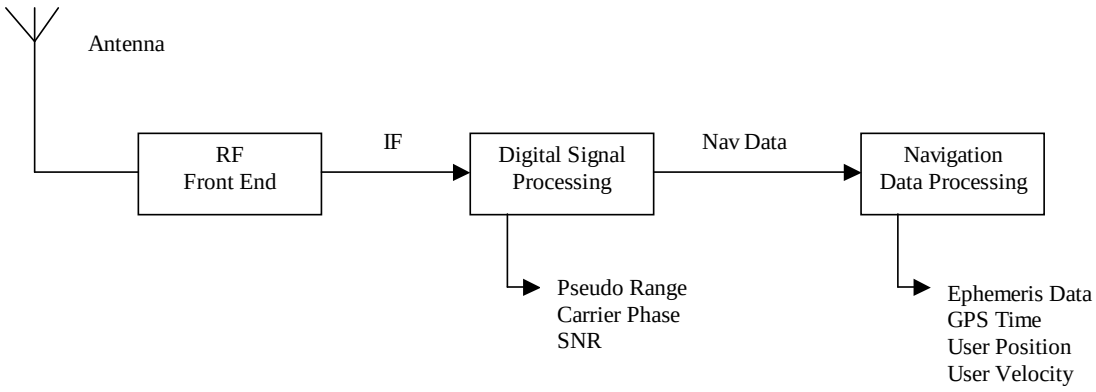

Fig. 4: Block diagram of a generic GPS receiver

The DSP performs the acquisition and tracking of the GPS signal. Traditional signal demodulation such as those used for FM or AM cannot be used for spread spectrum signals such as GPS because the signal level is below the noise level. Instead, the signal must be coherently integrated over time so that the noise is averaged out, thereby raising the signal above the noise floor.

Any GPS receiver locking up on a GPS satellite has to do a two-dimensional search for the signal. The first dimension is time. The GPS signal structure for each satellite consists of a 1023 bit long pseudo-random number (PRN) sequence sent at a rate of 1.023 megabits/sec, i.e. the code repeats every millisecond. To acquire in this dimension, the receiver needs to set an internal clock to the correct one of the 1023 possible time slots by trying all possible values. Once the correct delay is found, it is tracked with a Delay Lock Loop (DLL).

The second dimension is the frequency. The receiver must correct for inaccuracies in the apparent Doppler frequency. Once the carrier frequency is evaluated, it is tracked with a Phase Lock Loop (PLL). Figure 5 shows an extremely simplified PLL/DLL architecture. A more precise description of the GPS signal processing can be found in (Ward, 1996).

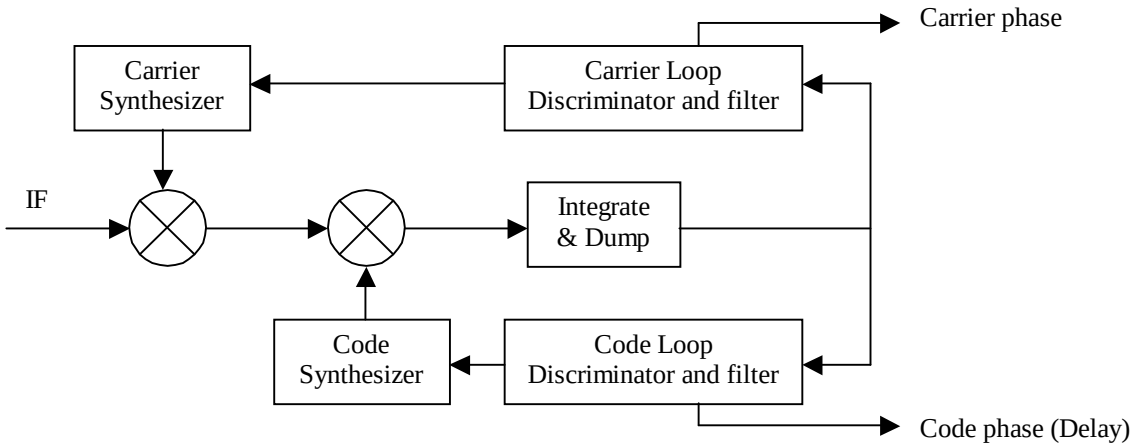

Fig. 5: Simplified GPS Digital Receiver Channel

6.2 Phase Noise at Receiver Level

When the receiver is unable to track the carrier phase, the signal is lost. Loss of lock is directly related with PLL cycle slips. To evaluate the occurrence of cycle slips, the tracking error variance at the output of the PLL has to be considered. Following (Conker, El Arini, 2003), this variance is expressed as a sum of three terms:

$$\sigma_{\Phi}^2 = \sigma_{\Phi S}^2 + \sigma_{\Phi T}^2 + \sigma_{\Phi,osc}^2 \quad (10)$$

where

$\sigma_{\Phi S}$ is the phase scintillation

$\sigma_{\Phi T}$ is the thermal noise

$\sigma_{\Phi,osc}$ is the receiver oscillator noise (0.122 rad)

The phase variance scintillation at the output of the PLL is given by :

$$\sigma_{\Phi S}^2 = \int_{-\infty}^{\infty} \left|1 - H(f)\right|^2 S_{\Phi}(f)\, df \quad (11)$$

where $S_{\Phi}(f)$ is the PSD of phase scintillation.

Figure 6 shows a phase scintillation spectrum obtained with GISM. $\left|1 - H(f)\right|^2$ is the closed loop transfer function of the PLL and depends on k, the loop order, and fn, the loop natural frequency. Typical values are k = 3 and fn = 1.91 Hz.

$$\left|1 - H(f)\right|^2 = \frac{f^{2k}}{f^{2k} + f_n^{2k}} \quad (12)$$

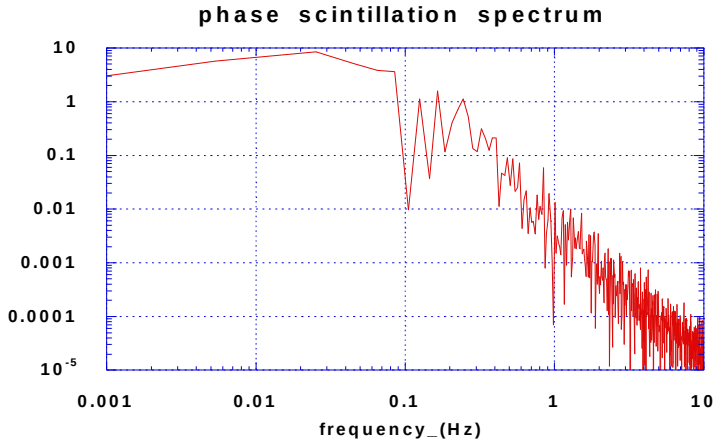

Fig. 6 : PSD of phase scintillation computed with GISM

When there is no scintillation, the standard thermal noise tracking error for the PLL is :

$$\sigma^2_{\Phi T} = \frac{B_n}{(c/n_0)}\left[1 + \frac{1}{2\eta\ (c/n_0)}\right] \quad (13)$$

where c/n0 is the signal to noise ratio (SNR), Bn is the receiver bandwidth, and η is the predetection time. For airborne GPS receiver, Bn = 10 Hz and η = 10 ms. Amplitude scintillation alters the SNR and increases the thermal noise tracking error. According to (Conker, El Arini, 2003), in presence of scintillation characterized by S4 index, thermal noise tracking error is given by :

$$\sigma^2_{\Phi T} = \frac{B_n\left[1 + \frac{1}{2\eta\ (c/n_0)\ (1 - 2\,S_4^2)}\right]}{(c/n_0)\ (1 - S_4^2)} \quad (14)$$

Equation (14) needs the evaluation of the SNR.
The GPS link budget can be expressed in dB as following :

$$C / N_0 = P_0 + Gt + Gr - \text{Propagation losses} - \text{Insertion Losses} - N_0 \quad (15)$$

where P_0 is the transmitted power, Gt and Gr are antenna gains of the transmitter and the receiver antenna, respectively, and N_0 is the receiver noise density. Therefore, the SNR appears to be depending on the elevation angle as shown in figure 7.

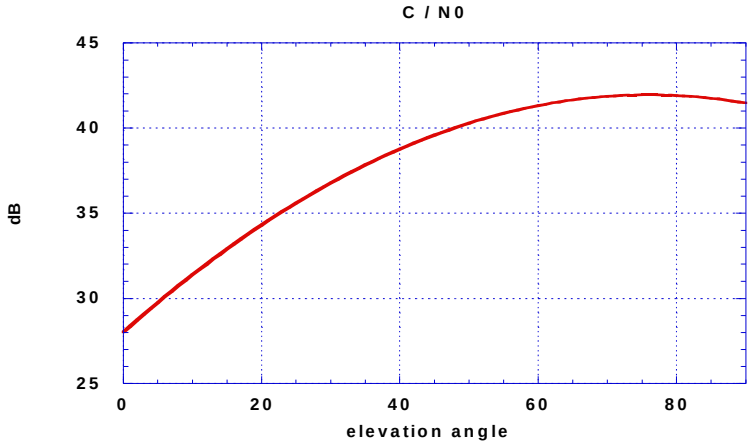

Figure 7: C/N_0 vs. elevation angle without scintillation for a GPS link

Equations (11) and (14) can be used to compute the PLL tracking error variance. Figure 8 is a comparison of this variance vs. C/N0 for S4 = 0.7 and S4 = 0.5. Loss of lock is highly probable for values above the 15° threshold. Therefore a receiver is able to tolerate scintillation if the C/N0 is above a minimum value. This minimum is 26 dB for S4 = 0.5 and 32 dB for S4 = 0.7.

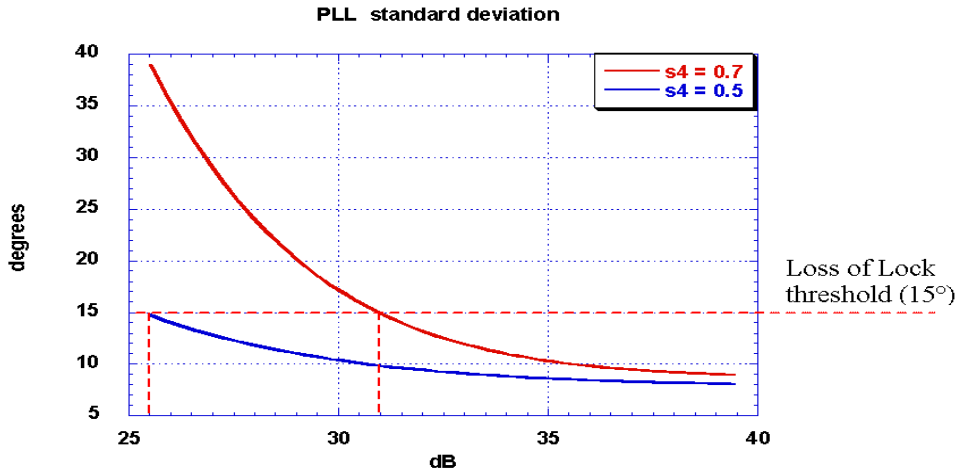

Figure 8: PLL standard deviation vs. C/N0

7. Loss of Lock Probability

Thermal noise appears to be the essential contribution to PLL tracking error. It is the unique S4 dependent term in (14) and the influence of S4 is shown on fig. 8. To calculate the Loss of lock probability, we consider the scintillation intensity and the related fades duration as presented on Figures 9 and 10, obtained by modelling.

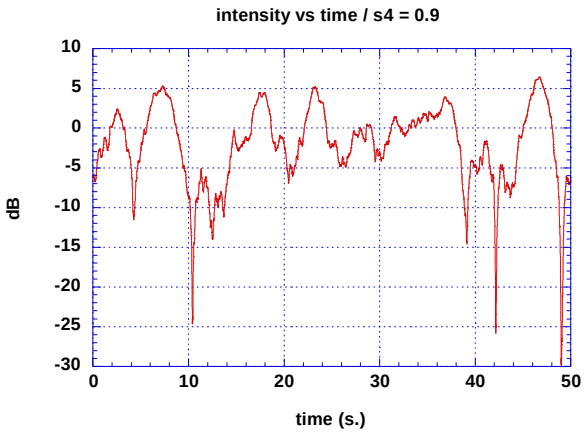

Figure 9: Scintillation intensity vs. time computed with GISM

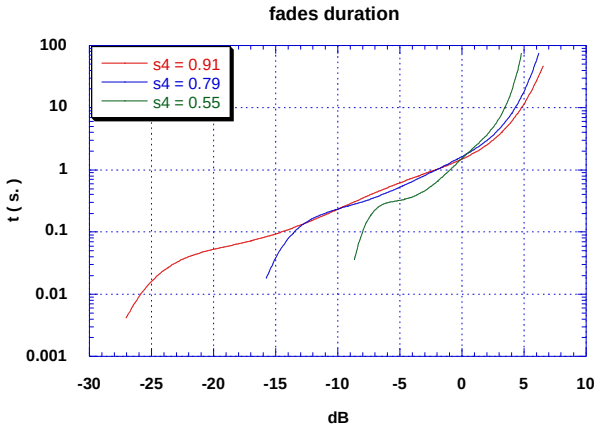

Figure 10: fades duration vs. fade depth

These plots have been obtained under severe scintillation conditions (S4 = 0.9). The corresponding fades duration always exceeds the pre integration duration time. As a consequence it corresponds to a degradation of the SNR at receiver level:

$$C/N = C/N0 + Is(\text{in dB}) \qquad (16)$$

or, with the fractional form:

$$c/n = c/n0 * Is \qquad (17)$$

where Is is the scintillation intensity of mean value equal to 1 and Nakagami distributed with parameter S4. Equation (14) is modified to take the fading into account:

$$\sigma^2_{\Phi T} = \frac{B_n}{(c/n_0)\ Is}\left[1 + \frac{1}{2\eta (c/n_0)\ Is}\right] \qquad (18)$$

This relation expresses the thermal noise as a decreasing function of the scintillation intensity. As a result, if $\sigma_{\Phi T}$ is above the 15° threshold then Is is below a value computed using (18). As Is distribution is known for a given S4, the probability of occurrence of "Is < threshold" can be evaluated. The result is the probability of Loss of Lock.

Figure 11 presents this probability versus S4 at given values of the SNR. It can be noticed that links with high SNR are quite robust. On the contrary, links with low values of SNR are likely to be lost.

GISM has an integrated GPS satellite trajectory generator. It has been used use to simulate a whole day (24th September 2001) over Naha (Japan, latitude = 26° geographic, 15° magnetic). All visible satellites were used to compute an average probability of loss of lock. The result is 0.21 %, i.e. each satellite was 0.21% of the time locked out during that day.

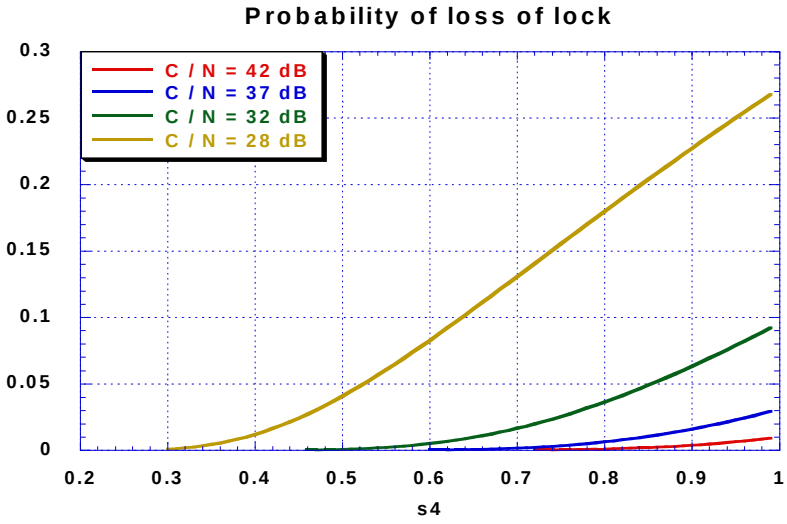

Figure 11: Probability of loss of lock vs. s4 for 4 values of the SNR

8. Positioning Errors

In most cases, scintillations don't affect all visible satellites. If the number of satellites is above 4 then a standard receiver should be able to provide navigation information. However, the number of satellites and their positions affect the positioning precision. The Dilution Of Precision (DOP) is usually used to quantify this precision. The DOP is related to the geometrical distribution of the visible constellation. The scheme on figure 12 shows how the DOP is related to the satellites positions. The DOP is used to derive the positioning error (σ_p) from the User Equivalent Range Error (UERE):

$$\sigma_p = DOP * UERE \quad (19)$$

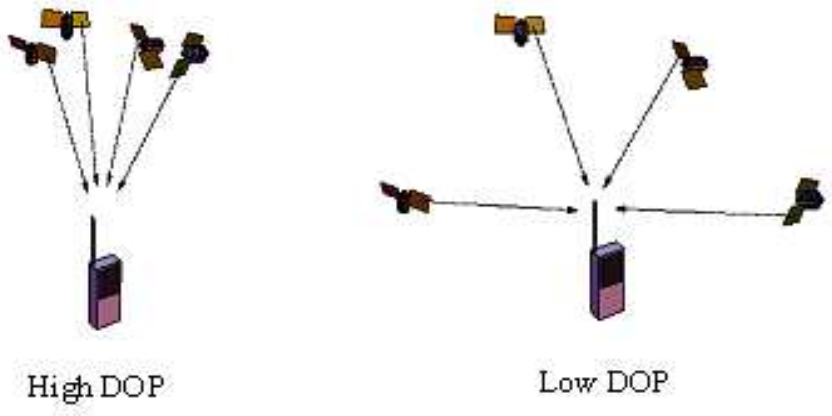

Figure 12: DOP and constellation

GISM was used to compute all scintillation parameters for each GPS satellite visible from Naha (Japan). The tracking error was derived from these parameters and from typical receiver characteristics. Satellites with tracking error above the 15° threshold were ignored for the DOP evaluation. Figure 13 presents the resulting DOP, compared with the DOP of the unaffected constellation. In worst cases, the DOP value obtained during scintillation can be twice the value obtained under normal conditions.

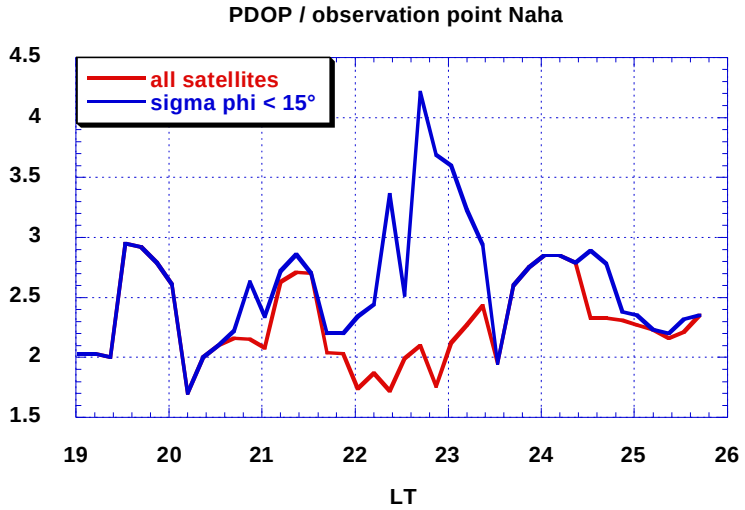

Figure 13: DOP at Naha under scintillation conditions computed with GISM

Even if the signal transmitted from a GPS satellite is not lost, it can alter the position precision. One of the DLL functions is the measurement of the delay between the code carried by the GPS signal and the receiver internal clock. This delay is an estimation of the time needed by the GPS signal to reach the receiver. The receiver is then able to compute the distance of the satellite. Errors in this estimation are collected in the UERE. To take into account the scintillations, we have to consider the DLL tracking errors.

The DLL can be studied like the PLL to evaluate its tracking error variance in degrees. The UERE due to scintillations can then be deduced with a product with the chip length (equal to 293 m for L1 (Conker, El Arini, 2003). The results are shown on Figure 14. These results show high degradation of the UERE. Satellites with high DLL tracking errors have also high PLL tracking errors and therefore they might be considered as lost and don't contribute to the UERE.

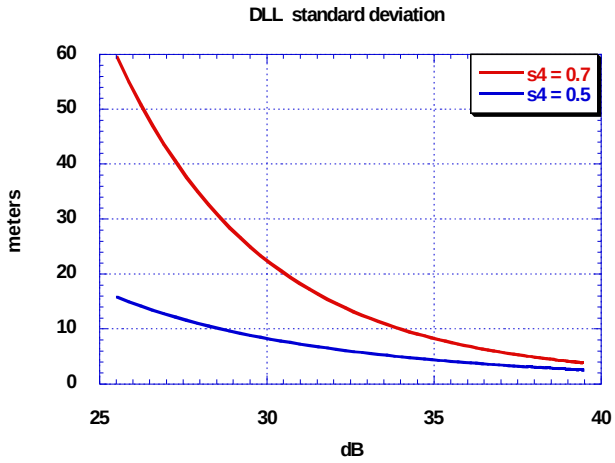

Figure 14: DLL tracking error

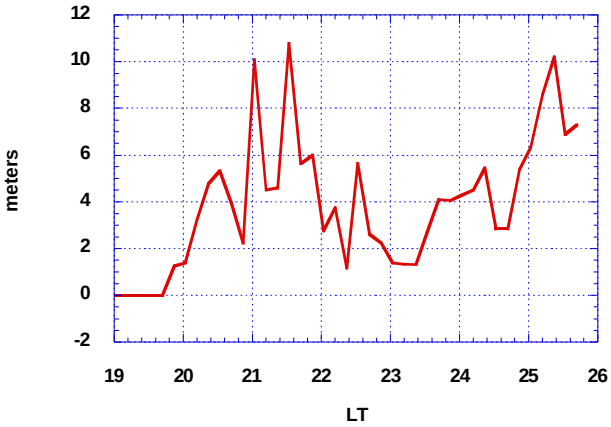

Figure 15: Positioning error at Naha (Japan) under scintillation conditions, computed with GISM

The combination of both effects is presented in Fig. 15. Satellites with PLL tracking errors above 15° were considered invisible for the DOP calculation. All other links with visible satellites were used to compute a mean UERE contribution due to scintillation.

9. Simultaneous Loss of Lock

Taking the 15° criteria for loss of lock threshold, the links with such a phase standard deviation level have been selected. This gives the number of satellites simultaneously locked out. The result is reported on figure 16. Three satellites may be lost simultaneously in a few cases, which correspond to the highest values of the DOP. As a comparison, the measurements results are presented on figure 17 (Matsunaga, 2002, El Arini, 2003). Locked out links are in brown. Three satellites are locked out simultaneously in some cases and even 4 in extreme cases.

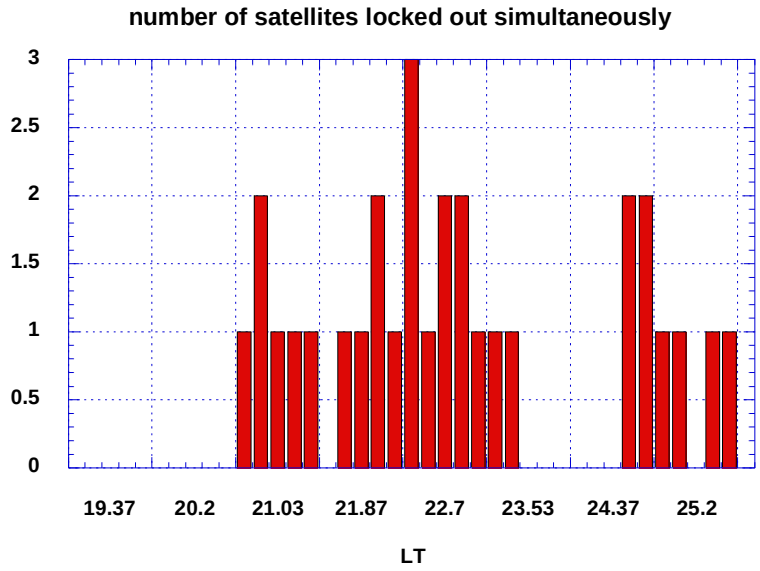

Figure 16: number of satellites locked out simultaneously with GISM

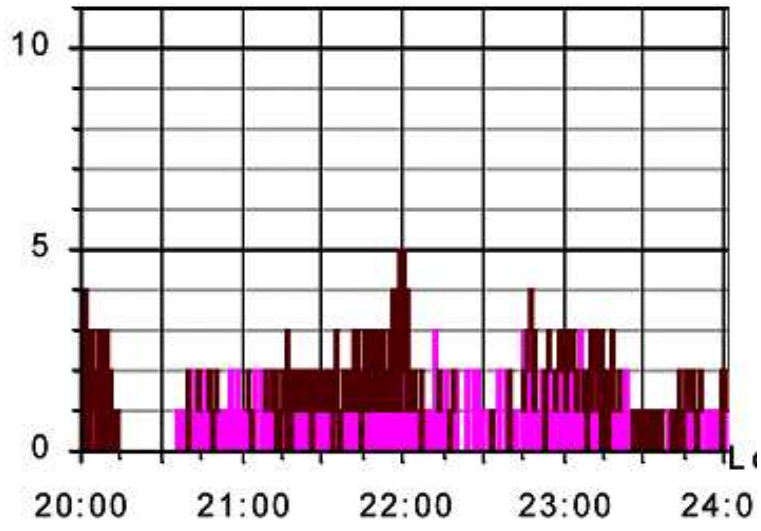

Figure 17: number of satellites locked out simultaneously (Measurements in Naha)

10. Comparisons Models results and measurements

The results reported hereafter are taken from the PRIS measurement campaign (Béniguel, 2009) carried out under ESA / ESTEC contract N° 19530. For this study, a number of receivers were deployed both at low and high latitudes, in particular in Vietnam, Indonesia, Guiana, Cameroon, Chad and Sweden. These receivers were dedicated receivers, operating at 50 Hz. A data bank has been constituted and the scintillation characteristics have been derived from an extensive analysis of this data bank. Comparisons between measurements and results provided by GISM model in the same conditions have been done both for the scintillation indices and the spectrum.

Scintillation indices

One week of measurements at Cayenne, French Guiana was selected. The results are presented on Figures 18. The x axis corresponds to local time at receiver location. The 0 value has been set arbitrarily to Saturday 19:00, the week of observation.

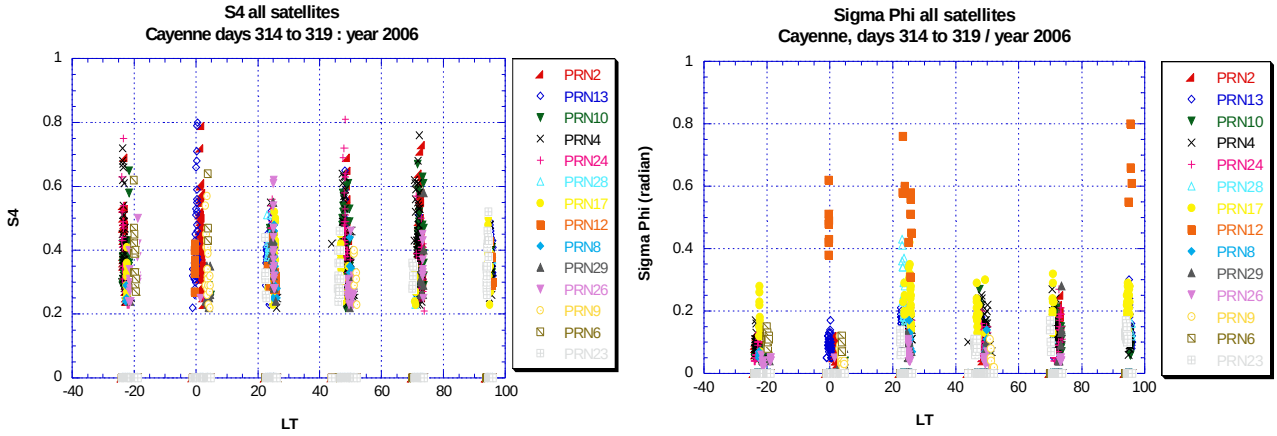

Figure 18: Intensity and phase scintillation indices measurements on GPS week N° 377

Measurements

The local time corresponds to hours in GPS time. Each point corresponds to a 1 minute sample. Only points with a S4 value greater than 0.2 were retained in the analysis. As can be seen on Figure 18, the points are clustered every evening at post sunset hours, typically 19:00 - 24:00. The scintillation activity occurred quite regularly that week with comparable levels. The S4 average value is about 0.4. The flux number that week (GPS week N° 377, modulo 1024) was equal to 90.

The phase fluctuations are plotted concurrently. The mean value is about 0.2, consequently lower than the S4 value. This observation is quite general. In addition, it has to be noticed that some points exhibit high values. Deep fades occur concurrently to these high values. In the case of very small values this creates phase jumps. As a consequence the phase and intensity standard deviations are no longer related.

Modelling

The scenario was replayed using the corresponding Yuma files for one particular day of the week (cf Figure 20). Another day will not bring significant differences considering that the geophysical parameters would have been quite identical. The flux number, input to GISM, has been set to 90. The model provides a mean value. It overestimates the number of affected links due to the fact that the probability of occurrence is not considered. Only the mean values can be compared. The scintillation intensity index mean value is about 0.4 corresponding to the measurements. The scintillation phase index mean value is slightly greater than the one recorded in the measurements. In both cases the phase RMS is lower than the intensity RMS and in both cases some points exhibit high values due to the phase jumps.

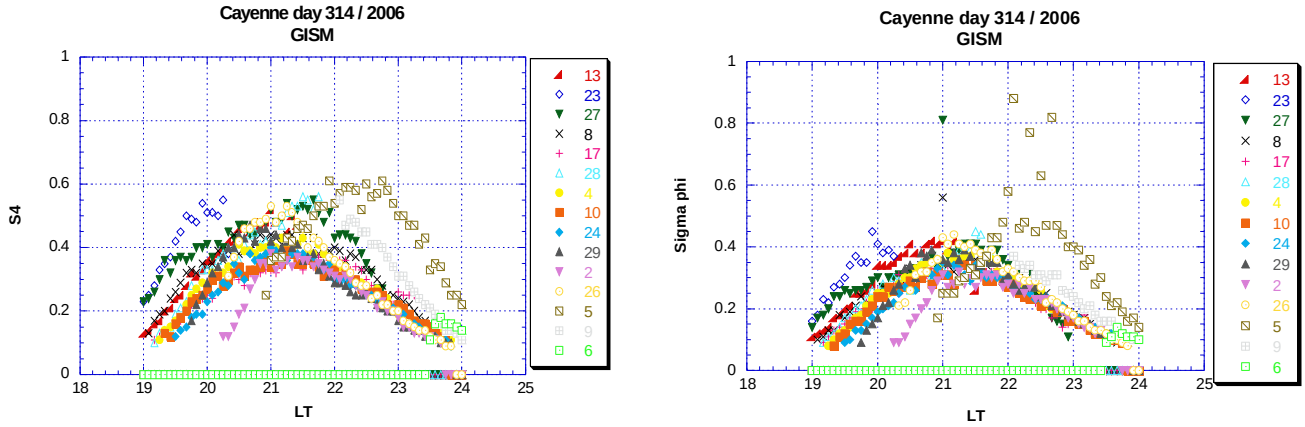

Figure 20: Intensity and phase scintillation indices on day 314, GPS week N° 377, obtained by modeling

11. References

[1] Aarons, J. "Global morphology of ionospheric scintillations" Proc. of the IEEE, 70 (4), 1982

[2] Afraimovitch, E. L., G. A. Zherentsov, V. N. Zverzdin, "Characteristics of small scale irregularities as deduced from scintillation observations of radio signals from satellites ETS-2 and Polar Bear at Irkutsk", Radio Science, vol. 29 (4), 1994

[3] Béniguel Y. "GIM: A Global Ionospheric Propagation Model for scintillations of transmitted signals", Radio Science, Vol **37 (3)**, 1032, doi:10.1029/2000RS002393, 2002

[4] Béniguel Y., J-P Adam, N. Jakowski, T. Noack, V. Wilken, J-J Valette, M. Cueto, A. Bourdillon, P. Lassudrie-Duchesne, B. Arbesser-Rastburg, Analysis of scintillation recorded during the PRIS measurement campaign, Radio Science, Vol **44**, doi:10.1029/2008RS004090, 2009

[5] Budden, K. G. "The propagation of radio waves", Cambridge University Press, ISBN 0-521-25461, 1985

[6] Conker, R. S., M. B. El-Arini, C. J. Hegarty, T. Hsiao, "Modeling the Effects of Ionospheric Scintillation on GPS/SBAS Availability", *Radio Science*, January/February 2003.

[7] Costa E., E. de Paula, L. Rezende, K. Groves, P. Roddy, E. Dao, M. Kelley, « Equatorial scintillation calculations based on coherent scatter radar and C/NOFS data, Radio Science, Vol **46**, doi :10.1029/2010RS004435, 2011

[8] El Arini B., R. Conker, Y. Béniguel, J-P Adam, "Comparing measured s4 with the calculated s4 by the WBMOD and GISM at Naha, Japan", SBAS Iono Meeeting, September 2003

[9] Gherm V., N. Zernov, H. Strangeways, Propagation model for transionospheric fluctuating paths of propagation: simulator of the transionospheric channel, Radio Science, Vol **40**, RS1003, doi:10.1029/2004RS003097, 2005

[10] Ishimaru A., Wave propagation and scattering in random media, Vol. **2**, Academic Press, ISBN 0-12-374702-3, 1978

[11] Knepp D., Multiple phase screen calculation of the temporal behavior of stochastic waves, Proceedindgs of the IEEE, Vol **71**, N° 6, 1983

[12] K. Matsunaga "Observation of Ionospheric Scintillations on GPS Signals in Japan", ION symposium, 2002

[13] Mc Dougall J. W., "Distributions of the irregularities which produce ionospheric scintillations" Journal of Atmospheric and Terrestrial Physics, vol. 43, 1981

[14] Picibono B. Introduction à l'étude des phénomènes aléatoires, Dunod, 1968

[15] Radicella S.M., The NeQuick model genesis, uses and evolution, Annals of Geophysics, Vol **52 (3-4)**, 2009.

[16] Rino C. L., A power law phase screen model for ionospheric scintillation, Radio Sci., Vol **14 (6)**, pp. 1135 – 1145, 1979.

[17] Yeh K. C., C. H. Liu, An investigation of temporal moments of stochastic waves, Radio Sci., Vol. **12 (5)**, pp. 671 - 680, Sept - Oct. 1977

[18] Ward, P. (1996), "Satellite Signal Acquisition and Tracking", *Understanding GPS Principles and Applications*, ed. E.D. Kaplan, Artech House, Boston, pp. 119-208.